Tribology International 131 (2019) 567–578

Contents lists available at ScienceDirect

Tribology International

journal homepage: www.elsevier.com/locate/triboint

Insights on low-friction mechanism of amorphous carbon films from reactive molecular dynamics study

Xiaowei Li[a,b,*], Aiying Wang[b], Kwang-Ryeol Lee[a,**]

[a] Computational Science Center, Korea Institute of Science and Technology, Seoul 136-791, Republic of Korea
[b] Key Laboratory of Marine Materials and Related Technologies, Zhejiang Key Laboratory of Marine Materials and Protective Technologies, Ningbo Institute of Materials Technology and Engineering, Chinese Academy of Sciences, Ningbo 315201, PR China

ARTICLE INFO

Keywords:
Friction behavior
Amorphous carbon
Passivation or graphitization mechanism
Reactive molecular dynamics

ABSTRACT

The dependence of friction behaviors of the self-mated a-C system on sliding velocity, *v*, and contact pressure, *P*, was investigated systematically by reactive molecular dynamics simulation. Results demonstrated that the friction coefficient and sp^3-to-sp^2 transformation of interfacial structure were more sensitive to the contact pressure than the sliding velocity. By analyzing the relation of friction coefficient and interfacial hybridization structure with *P*/*v* ratio, it suggested that the low friction coefficient, which was accompanied by the low sp^2 fraction, was strongly dependent on the passivation of friction interface as the primary mechanism. These findings disclose the proof for passivation mechanism mentioned in previous experiments, and also provide the potential strategy to fabricate new nanocomposite a-C films by surface/interface modification for tribo-applications.

1. Introduction

Amorphous carbon (a-C) film draws long-term attention from carbon community in both the scientific and engineering aspects because of the high hardness, low friction coefficient, chemical inertness, good biocompatibility, and optical transparency [1–3]. Most importantly, due to the growing energy and environment issues, by utilizing its unique friction properties, a-C film has been a strong candidate to improve the friction and wear properties and thus extend the lifetime of moving mechanical components, such as automotive fuel injection components, gears, tappets, cutting tools, etc [4]. As known that the complexity and diversity of friction mechanism for a-C film are strongly related with the friction condition, and many attempts also have been launched to reveal the underlying low-friction mechanism of a-C film by probing the dependence of friction on normal load [5], sliding velocity [6], environmental condition [7], and counterpart material [8].

So far, two best-known theories for the low friction are the friction-induced structural graphitization [9–12] and passivation of carbon dangling bonds induced by chemical termination [13–15] or rehybridization [16,17] at the sliding interface. Among of them, the graphitization mechanism is commonly followed by both the increased fraction and ordered lamellar structure of sp^2 phase, which has been more widely adopted to explain the experimental results [9–12]. The argument is that although most of previous experiments [5,18,19] about graphitization mechanism disclosed the increased fraction of sp^2-hybridized structure, the typical lamellar characteristics are seldom found. Hence, these structures are far from the crystalline graphite and cannot imitate the easy shearing behavior of graphite. Especially, Chen et al. [13] recently reported that the graphitized lamellar structure was distinguished by the state-of-the-art microscopy technique, but the ultralow friction was only achieved in the surface-passivated system. Cui et al. [14] also clarified that the friction was primarily affected by the adsorption of passivating gas to the sliding surface rather than the graphitization degree of a-C surface, supporting the passivation of carbon dangling bonds as the primary friction mechanism of a-C films. However, when two surfaces slide past each other, our understanding on the atomistic processing occurring at the friction interfaces is still quite limited due to the complexity of structural evolution of friction interface. Especially, the characterization of un-passivated hybridized bonds is still not accessible by experiment, inducing the friction mechanism limited to the phenomenal rather than the fundamental understanding, while it is essential to reveal the intrinsic mechanism ruling the sliding friction.

In the present work, we performed the reactive force field molecular dynamics (RMD) simulation to evaluate the friction behavior of self-mated a-C films (a-C/a-C), in which the passivation of H on a-C surface

* Corresponding author. Computational Science Center, Korea Institute of Science and Technology, Seoul 136-791, Republic of Korea.
** Corresponding author.
E-mail addresses: lixw0826@gmail.com (X. Li), krlee@kist.re.kr (K.-R. Lee).

https://doi.org/10.1016/j.triboint.2018.11.021
Received 19 September 2018; Received in revised form 30 October 2018; Accepted 20 November 2018
Available online 20 November 2018
0301-679X/ © 2018 Elsevier Ltd. All rights reserved.

was excluded in order to clarify the real nature of friction in intrinsic a-C films and eliminate the effect of H on mechanical properties [20]. The new developed ReaxFF potential [21,22] was used to describe the complicated C—C interaction during the friction process. This potential is based on the bond order concept to consider the instantaneous interactions between atoms and gives more accurate description for the carbon bond formation and dissociation than previous empirical potentials (Tersoff [23,24], REBO [25], and AIREBO [26]). To the best of our knowledge, there is also no published work on the friction simulation of a-C films from the atomic scale using ReaxFF. The effect of sliding velocity and contact pressure on the friction properties was systematically investigated and the corresponding evolution of interfacial structure was mainly focused. Results revealed that friction property strongly depended on the sliding velocity and contact pressure, and the low friction was mainly dominated by the passivation of friction interface.

2. Computational methods

2.1. Models and parameters

RMD simulation was adopted to study the friction process of a-C/a-C system using the Large-scale Atomic/Molecular Massively Parallel Simulator (LAMMPS) code [27]. As shown in Fig. 1, the a-C structure with size of 42.88 × 40.358 × 31 Å^3, sp^3 fraction of 24 at.%, and sp^2 fraction of 72 at.% was chosen as the bottom and upper mating material, which was produced by atom-by-atom method and composed of 6877 carbon atoms. The detailed deposition process could be found in our previous work [28]. The atoms in the bottom and upper thickness of 5 Å along the z direction were fixed to mimic the semi-infinite large surface. Temperature of the neighboring thickness of 5 Å in the bottom and upper mating a-C structures was coupled to 300 K by Berendsen thermostat [29] with a damping constant 100 fs to provide a thermal reservoir. All remaining atoms were completely unconstrained and free to simulate the structural evolution during the friction process. Initial separation between the bottom and upper mating a-C systems was 3 Å. The process was simulated using *NVE* ensemble implemented in LAMMPS code. Periodic boundary condition was employed along *x* and *y* directions and a MD time step of 0.25 fs was used.

Before the friction process, the geometry optimization (GO) for a-C/a-C friction system was first conducted at 300 K for 2.5 ps, and then the external pressure was applied to the top rigid layer during 25 ps to reach the desired values of 5, 20, or 50 GPa, respectively. The high contact pressure, which could be possible for instantaneous contact of a-C asperities during friction process [16,30–33], was appropriate for examining the friction behavior on an atomic scale. After that, the sliding process was undertaken along the *x* direction by exerting the sliding velocity (*v*) ranged from 1 to 10 and 30 m/s on the upper fixed a-C layer. The sliding process lasted 1.25 ns for 10 and 30 m/s and 5.695 ns for 1 m/s separately to get the steady-state friction stage. After friction process, the friction coefficient (μ) was calculated using the following equation:

$$\mu = \frac{f}{W} \tag{1}$$

where, the frictional force, *f*, and the load, *W*, were calculated by summing the force acting on the fixed atoms of bottom a-C layer in the *x* and *z* directions, respectively.

2.2. ReaxFF validation

Based on the ReaxFF force field developed by Srinivasan [21], the version revised by Tavazza [22] was used in the present work to describe the C—C interaction, which includes the covalent terms, coulomb interactions, dispersion, and other non-bonding forces. Although it has been confirmed to model covalent bond forming and breaking, rehybridization and chemical reactions accurately in carbon-based structures, the additional evaluations including the fabrication of a-C structure using quenching method [34,35], energy change induced by expansion and compressions, and temperature dependence of formation energy of a-C structure were further undertaken by ReaxFF MD and ab-initio calculations [36,37] separately to validate the reliability of the used force field, as shown in Fig. 2. It clearly revealed that the sp^3 fraction-density relationship (Fig. 2a) was well reproduced compared to our and previous DFT calculations [38–41] and experiment results [42,43], and the energy changes as a function of box volume (Fig. 2b) and temperature (Fig. 2c) were also in accordance with that from ab-initio calculations, which verified the validity of the force field for our simulated a-C system. Moreover, the growth simulations of a-C film were also performed by atom-by-atom approach, revealing that compared to the results using widely accepted AIREBO potential [26], the ReaxFF also gave the reasonable values of density, hybridization ratio, biaxial stress, radical distribution function, and bond angle and length distributions of a-C structure.

3. Results and discussion

3.1. Dependence of friction behavior of a-C/a-C system on the sliding velocity

The effect of different sliding velocities on the friction behavior of a-C/a-C system is examined first, and the contact pressure is fixed at 5 GPa. Fig. 3 shows the change of morphologies as a function of sliding time for each case. It can be seen that during the friction process, the

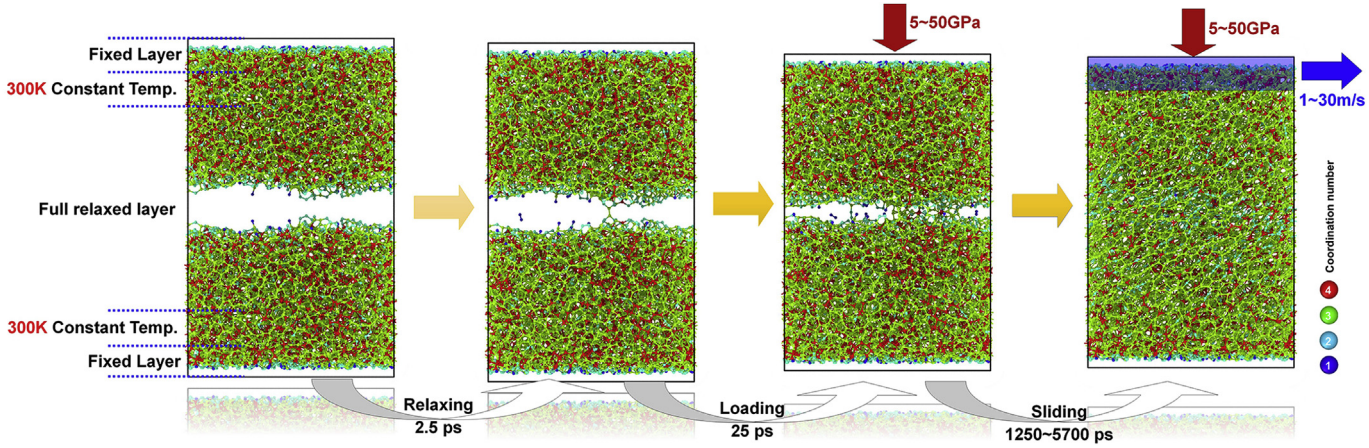

Fig. 1. Friction simulation model and related parameters.

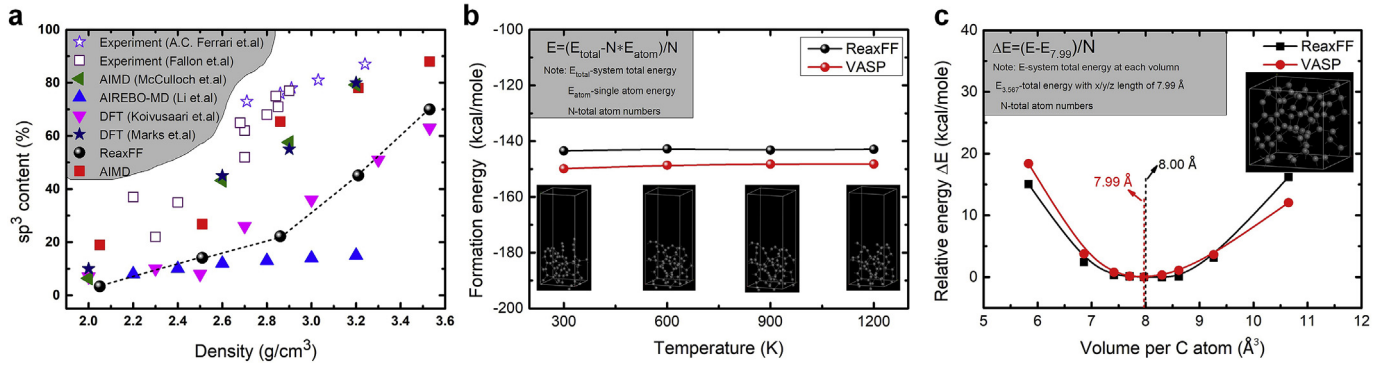

Fig. 2. Validation for the used ReaxFF force field in a-C system including (a) a-C structure fabrication using quenching method, (b) energy change induced by expansion and compressions, and (c) temperature dependence of formation energy of a-C structure. The results were compared with our and previous DFT calculations [38–41] and experiment results [42,43].

atoms from both bottom and upper a-C surfaces interact with each other to form the stable friction interface, and the coordination number of C atoms with sliding time changes gradually, implying the evolution of structural properties, as will be discussed later. In addition, with the sliding velocity increased from 1 to 30 m/s, the time spent for running-in process decreases, which is confirmed by the energy variations including kinetic (KE) and potential energies (PE), as shown in Fig. 4a. For each case, the temperature with sliding time increases first and then becomes stable following the aggravated fluctuation; the average temperatures during the stable friction stage are 306 ± 3 K for 1 m/s,

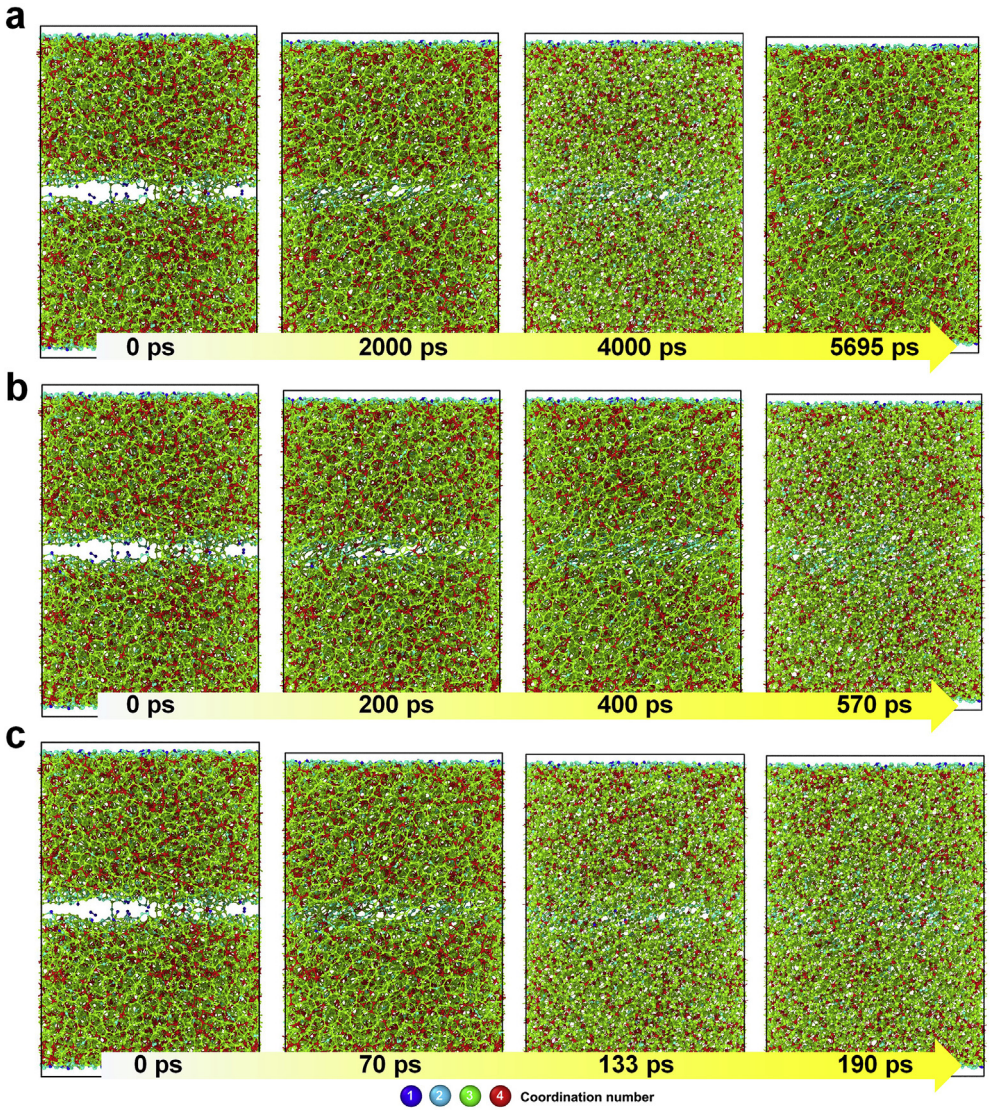

Fig. 3. Morphologies of a-C/a-C friction systems with sliding time under sliding velocities of (a) 1, (b) 10 and (c) 30 m/s, respectively.

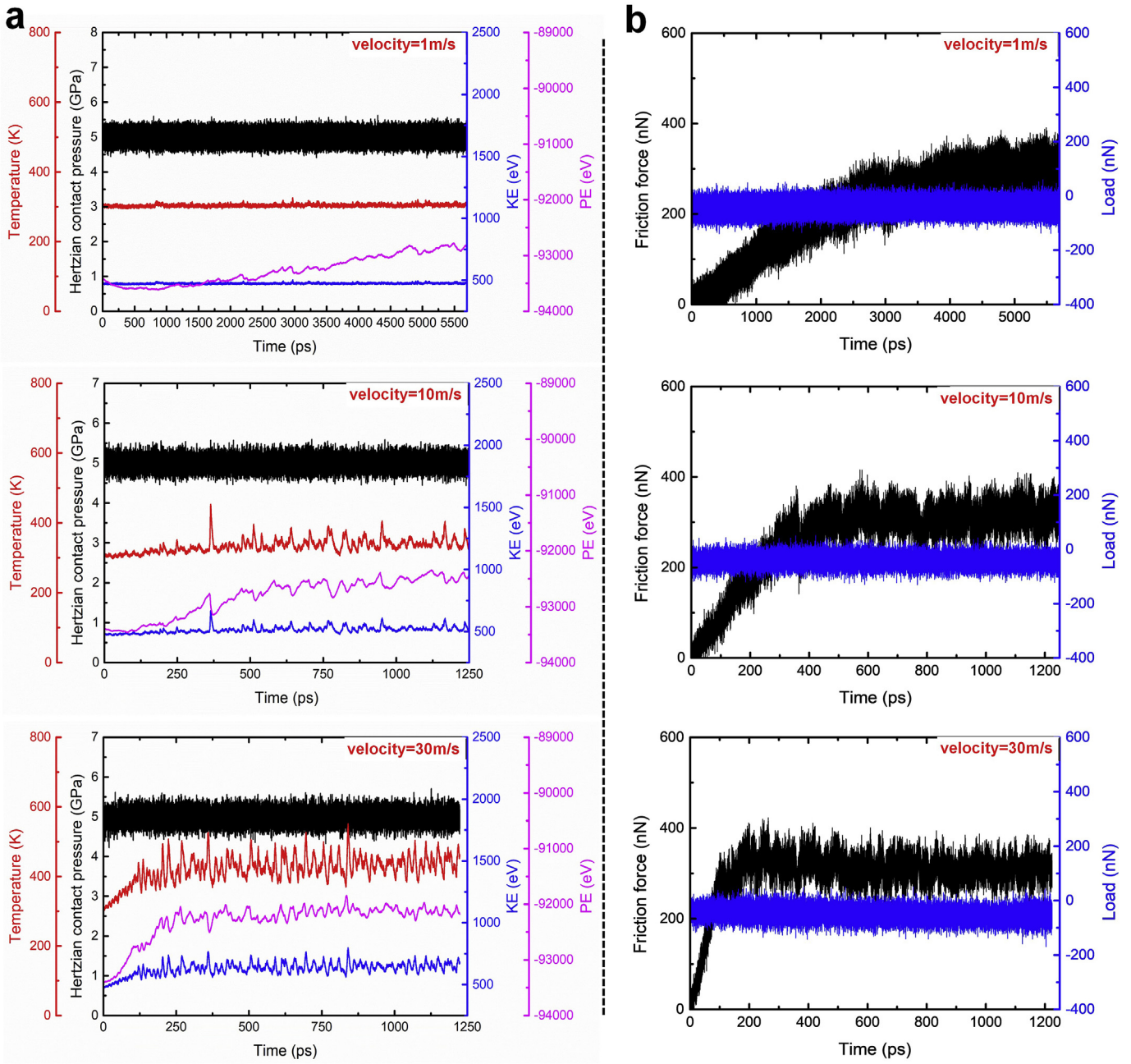

Fig. 4. (a) Contact pressure, temperature, KE and PE with sliding time under different sliding velocities (1–30 m/s). (b) Friction results including friction force and load curves with sliding time under different sliding velocities (1–30 m/s).

344 ± 14 K for 10 m/s, and 441 ± 25 K for 30 m/s, respectively. This change is related with the rate of corresponding heat generation per unit area at the contact, q, which can be evaluated as following [44].

$$q = \frac{\mu W v}{A} = \frac{f v}{A} \tag{2}$$

where A is the real contact area, μ is the friction coefficient, W is the applied normal load, v is the sliding velocity, and f is the friction force. Therefore, both sliding velocity and friction force contribute to the local rise of temperature at the contact interface.

As the sliding velocity increases from 1 to 30 m/s, the corresponding friction results including friction force and load curves with sliding time are illustrated in Fig. 4b. It further proves the presence of steady-state friction process, which is consistent with the energy changes (Fig. 4a). In order to evaluate the dependence of friction property on the sliding velocity, the friction force and load values during the last 200 ps are selected to calculate the average friction force and load. First, when the sliding velocity ranges from 1 to 30 m/s, the different load values, increased from 41 ± 31 to 54 ± 35 nN, are observed, which originates from the difference in real contact areas for each case according to the Hertzian contact theory. However, the friction force with sliding velocity only changes from 299 ± 31 to 310 ± 27 nN, suggesting that the obvious rise of temperature in Fig. 4a mainly attributes to the high sliding velocity according to Eq. (2) since increasing velocity means more energy applied to the system in a small amount of time. The steady-state friction coefficient is calculated for each case, as given in Fig. 5, displaying that the friction coefficient as a function of sliding velocity decreases. This is in agreement with previous experimental result [5]. However, note that although the friction coefficient values are close to previous report with the similar order [30], they are much

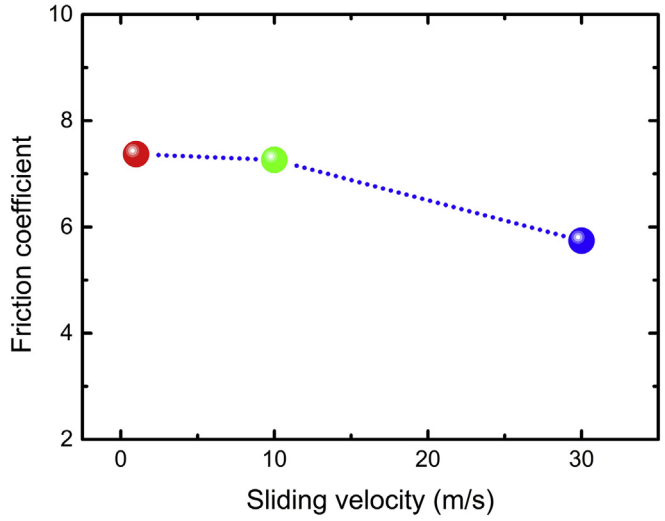

Fig. 5. Friction coefficient as a function of sliding velocity after friction process.

larger than experimental values, attributing to the strong adhesive strength between the two contact surfaces without any passivation or contamination estimated in experiment. In addition, it is also contributed by the difference in quantifying the real contact area accurately from experimental and simulation approaches.

In order to clarify the relation between the friction coefficient and sliding velocity, the corresponding evolution of structural property is required. Fig. 6 gives the time dependence of structural property distributions along the film depth direction when the sliding velocity is 30 m/s. It reveals that for each case, the whole system is divided into interfacial (gray color in Fig. 6), upper and bottom intrinsic a-C regions (white color in Fig. 6). Especially for the interfacial region, the obvious sharp interface exists before the sliding process and then disappears to form the intermixing layer with sliding time elapsed from 0 to 1250 ps. This attributes to the diffusion and rehybridization of interfacial C atoms, which is accompanied by the significant evolutions of density, biaxial stress, and coordination number. In order to quantify the changes in density, biaxial stress, and hybridization structure of each region, the specified thickness, such as 13.5 Å for interface (gray color in Figs. 6), 12 Å for bottom intrinsic a-C (left white color in Figs. 6), and 12 Å for upper intrinsic a-C (right white color in Fig. 6) are selected separately for each friction system. Taking the case under sling velocity of 30 m/s for example, the calculated results for each region are shown in Fig. 7. Note that for the interfacial region, the density and sp^2 fraction with sliding time increase obviously following the reduction of sp^3 fraction, while the fraction of 1-coordinated carbon atoms (denoted as s) is negligible; in particular, the biaxial stress transits from compressive to tensile state with high value. For the upper or bottom intrinsic a-C region, the density with sliding time decreases slightly, but the similar behaviors for biaxial stress and hybridization structure to those at interfacial region can be observed.

Fig. 8 further illustrates the dependence of density, biaxial stress, and hybridization fractions on sliding velocity after the friction process. The results after GO and loading process are also given for comparison. First, for the bottom and upper intrinsic a-C regions, there are similar changes in the biaxial stress, density, and hybridization structure; with increasing the sliding velocity from 1 to 30 m/s, the density,

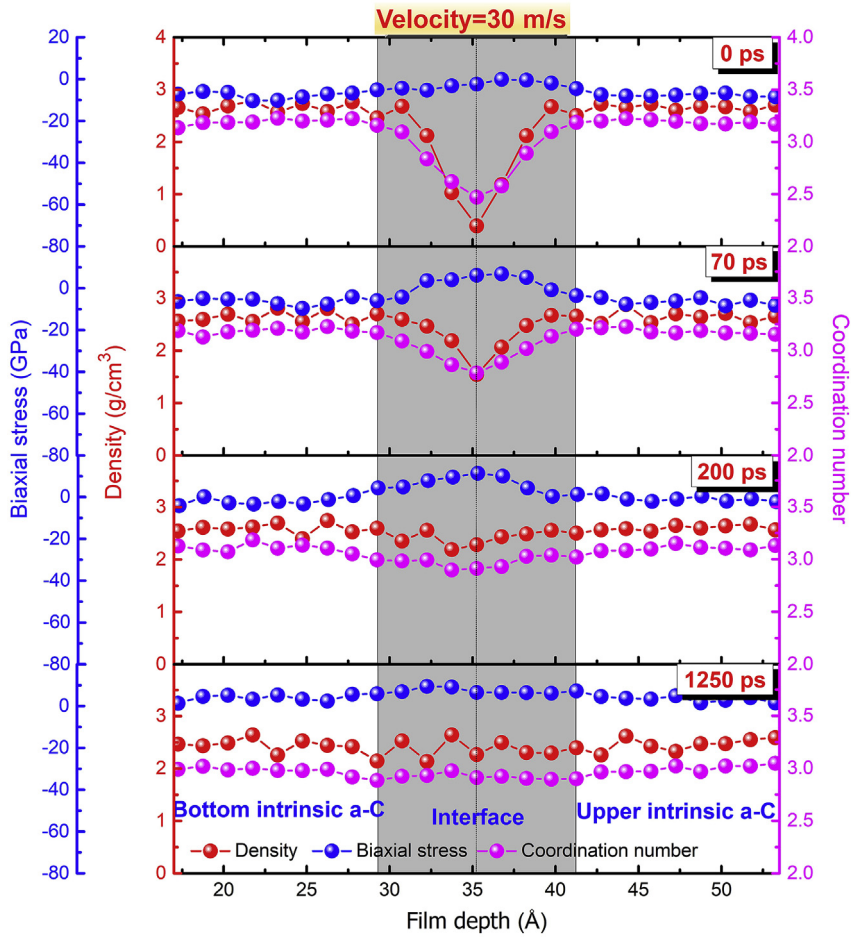

Fig. 6. Time dependence of structural property distributions along the film depth direction for the system under the sliding velocity of 30 m/s.

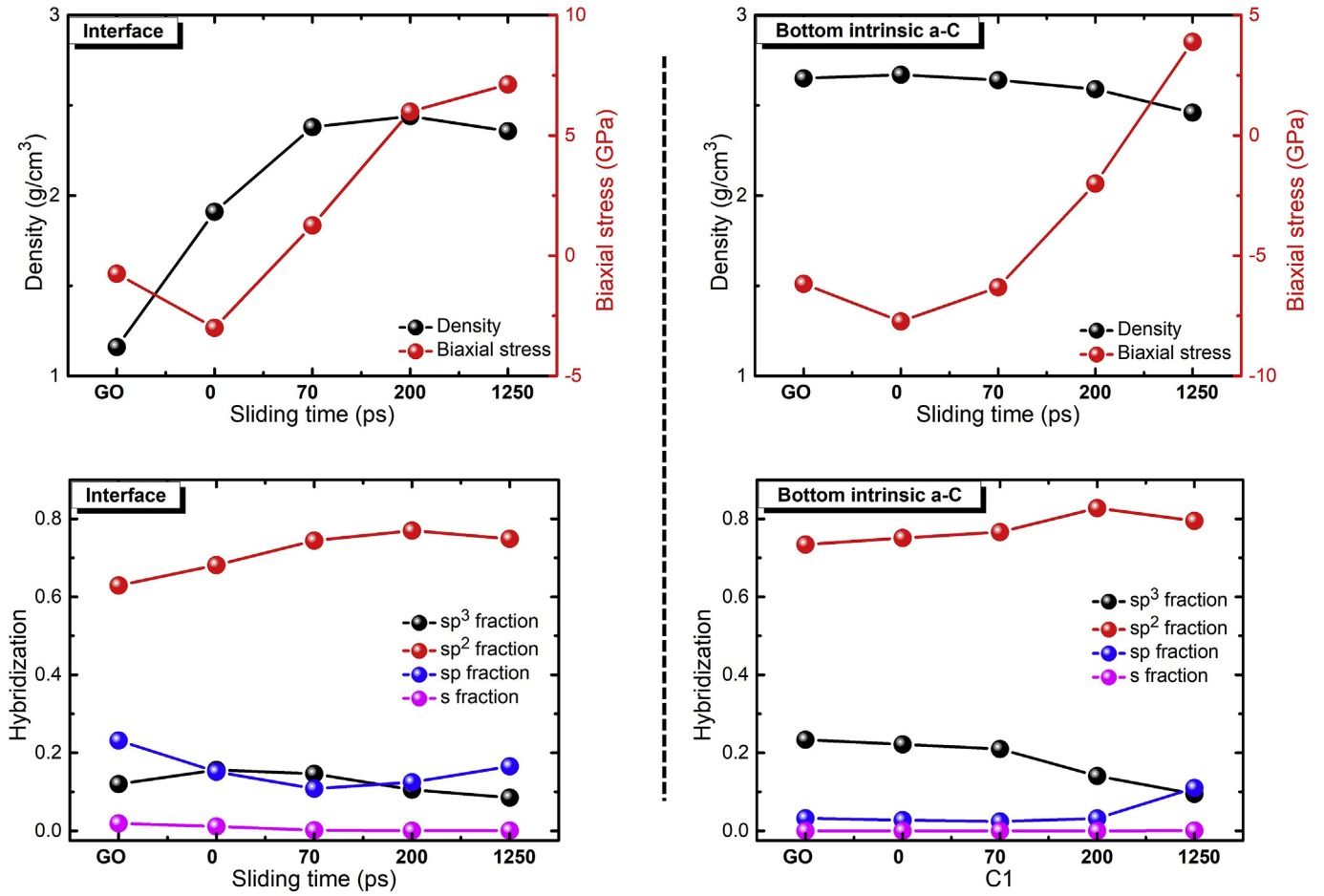

Fig. 7. Evolutions of the density, biaxial stress, and hybridization of interfacial and bottom intrinsic a-C regions with sliding time under the sliding velocity of 30 m/s, in which the results after GO are also given for comparison.

compressive stress, sp^3 and sp^2 fractions decrease following the increased sp fraction. For the interfacial region, the density with sliding velocity has slight change, but the hybridization structure also shows the similar behavior to that in intrinsic a-C region. Moreover, compared to the original structures after GO and loading processes, the increased sp^2 fraction is observed for each case after the friction process, suggesting the occurrence of sp^3-to-sp^2 transformation reported in experiments [5,18,19]. However, the sp^2 fraction with sliding velocity decreases, which is consistent with the change of friction coefficient. This demonstrates that the low friction coefficient is accompanied by the low sp^2 fraction. Kim et al. [5] reported that the decreased friction coefficient with sliding velocity attributed to the improved structural graphitization. This is not consistent with our present result, which subverts the friction-induced graphitization mechanism [9–12]. One of the main problems may be the limited experimental characterization, which cannot evaluate the carbon hybridized structure accurately and directly, leading to the controversy over the real nature of low friction.

3.2. Dependence of friction behavior of a-C/a-C system on the contact pressure

As is well known that the normal load also has serious effect on contacting state between the two sliding surfaces [5,14], so the corresponding friction behavior and structural properties are investigated by tailoring the contact pressure from 5 to 20 and 50 GPa, while the sliding velocity is fixed at 10 m/s. The friction results for the systems under the contact pressures of 20 and 50 GPa, respectively, are illustrated in Fig. 9. The morphologies display that because of the increase of contact pressure, the surface atoms from bottom and upper a-C films interact and mix with each other seriously. In particular, there is a distinct difference in coordination number evolution of C atoms for each case. When the contact pressure is 5 GPa, the sp^3 fraction with sliding time decrease gradually (Fig. 7), but it shows the contrary behavior obviously for the system under 50 GPa, implying the diverse structure transformation during the friction process, as will be discussed later.

Both the KE and PE variations with sliding time (Fig. 10) reveal that when the contact pressure is small, it will take longer time for running-in process to reach the stable friction stage due to the weak interfacial interaction. In addition, with increasing the contact pressure from 5 to 20 and 50 GPa, the temperature during the stable friction process increases from 344 ± 14 to 361 ± 14 and 439 ± 23 K separately. According to Eq. (2), the rise of temperatures originates from the increased friction force because of the fixed sliding velocity, which is confirmed by the friction force curves for each case, as illustrated in Fig. 10.

The friction force and load values during the last 200 ps of friction process (Fig. 10) are also adopted to calculate the friction coefficient for evaluating the effect of contact pressure on the friction property, as given in Fig. 11. Although the friction force with contact pressure increases significantly, but it is still slower than the increase of load, leading to the significant reduction of friction coefficient with contact pressure, which also agrees well with Kim's experimental result [5]; when the contact pressure is 50 GPa, the lowest friction coefficient of 0.57 is obtained, but it is still higher than the experimental value due to the non-contaminated friction surface.

Similar to the cases under different sliding velocities, the a-C/a-C

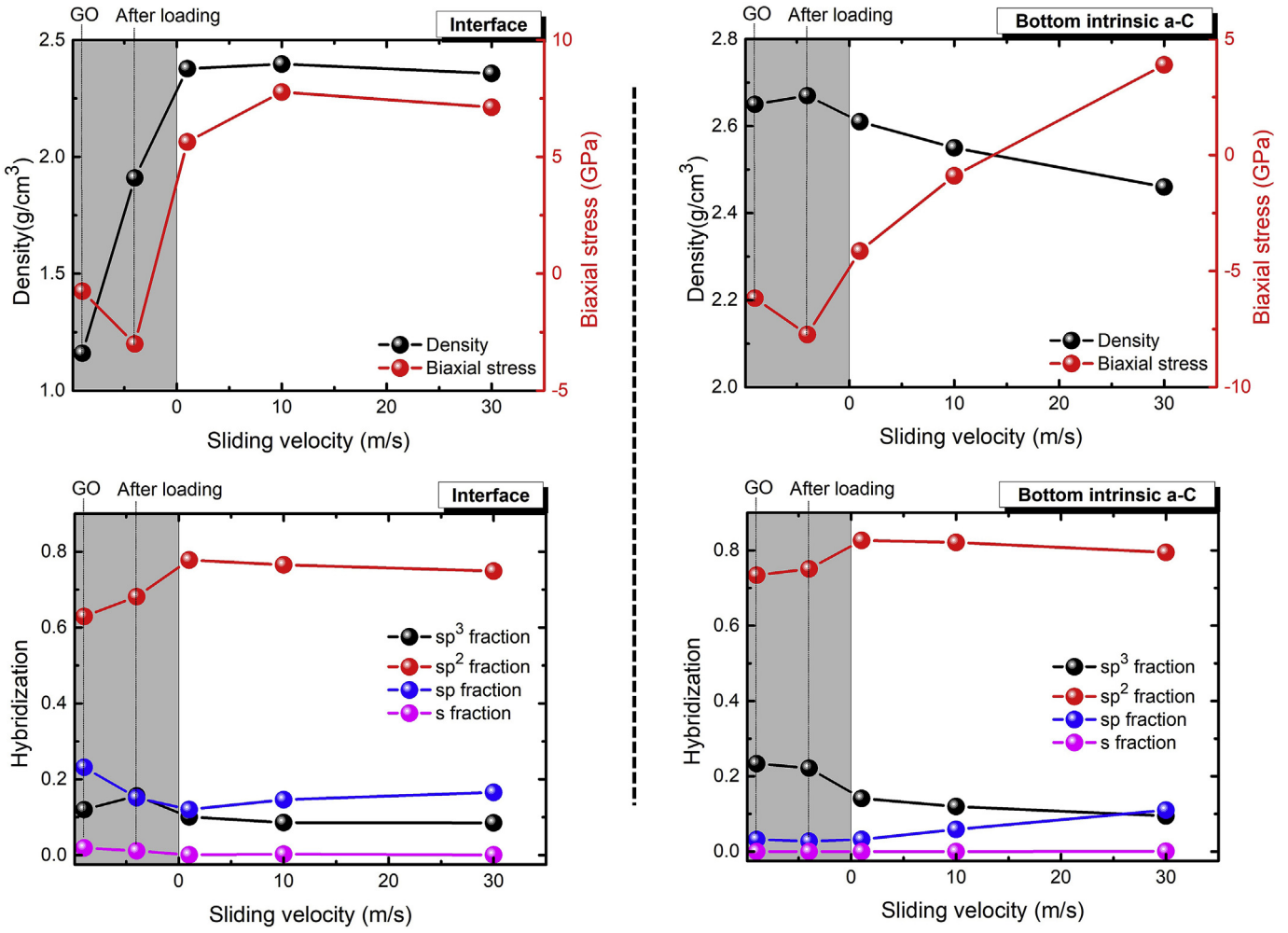

Fig. 8. Dependence of the density, biaxial stress, and hybridization of bottom intrinsic a-C and interfacial regions on sliding velocity after friction process, in which the results after GO and loading process are also given separately for comparison.

friction system under different contact pressures can be also divided into three regions, and thus the structure and properties of each region as a function of sliding time and contact pressure are quantified separately for each case. First, compared to the cases under different sliding velocities, the different evolution of structural properties with sliding time can be observed clearly when the contact pressure increases from 5 to 50 GPa. Taking the result under 50 GPa for example (Fig. 12), the density, compressive stress, and sp^3 fraction as a function of sliding time increase obviously for each region, which is accompanied by the reduction of sp^2 and sp fractions, suggesting the occurrence of friction-induced sp^2-to-sp^3 and sp-to-sp^3 transformations.

Fig. 13 gives the dependence of the density, biaxial stress, and hybridization structure on contact pressure after friction process. It reveals that with increasing the contact pressure from 5 to 50 GPa, the structure and properties in bottom and upper intrinsic a-C regions show the similar behaviors to those at interfacial region; the density, compressive stress, and sp^3 fraction with contact pressure increase, while the sp^2 and sp fractions reduce, indicating the pressure-driven sp^2-to-sp^3 and sp-to-sp^3 transformations. Compared to original structures after GO, the increased sp^2 fraction can only be achieved in the system under the contact pressure of 5 and 20 GPa. However, when the contact pressure further reaches to 50 GPa, the sp^2 fraction decreases obviously with the significant increase of sp^3 fraction (Fig. 13), while the minimal friction coefficient is obtained. This is highly consistent with the previous experiment reported by Cui et al. [14], which also cannot be interpreted by the friction-induced graphitization mechanism.

3.3. Discussion for friction mechanism

The above-mentioned results in Figs. 8 and 13 indicate that compared to the pristine a-C film, the sp^2 fraction could be enhanced, but it mainly depends on the contact pressure (Fig. 13). In particular, the friction coefficient with sliding velocity or contact pressure decreases without accompanying the enhanced sp^2 fraction at the interface. On the contrary, a higher friction coefficient is followed by a higher sp^2 fraction, which is also reported by Cui et al. in experiment [14]. Hence, the friction-induced graphitization mechanism is not suitable to clarify our present results.

According to the pressure-temperature (*P-T*) phase diagram for carbon [9,45], not only the temperature rise, but also a pressure decrease could induce the sp^3-to-sp^2 transition. For the increased sp^2 fraction in the present work, our results in Figs. 4 and 10 confirm that there is no high temperature generated during the friction process. Fig. 14a shows the relation of biaxial stress, temperature, and sp^2 fraction at the interfacial region after the friction process. It reveals that the sp^3-to-sp^2 transformation of hybridization structure primarily depends on the local stress condition, and the highly compressive stress favors the formation of a sp^3-rich phase (such as 50 GPa–10 m/s), while a tensile one favors a sp^2-rich phase (such as 5 GPa–30 m/s), which conforms to McKenzie's report [45].

Figs. 5 and 11 illustrate that the friction coefficient is strongly dependent on both the sliding velocity and contact pressure. In addition, previous experimental studies [14,46] reported that the friction

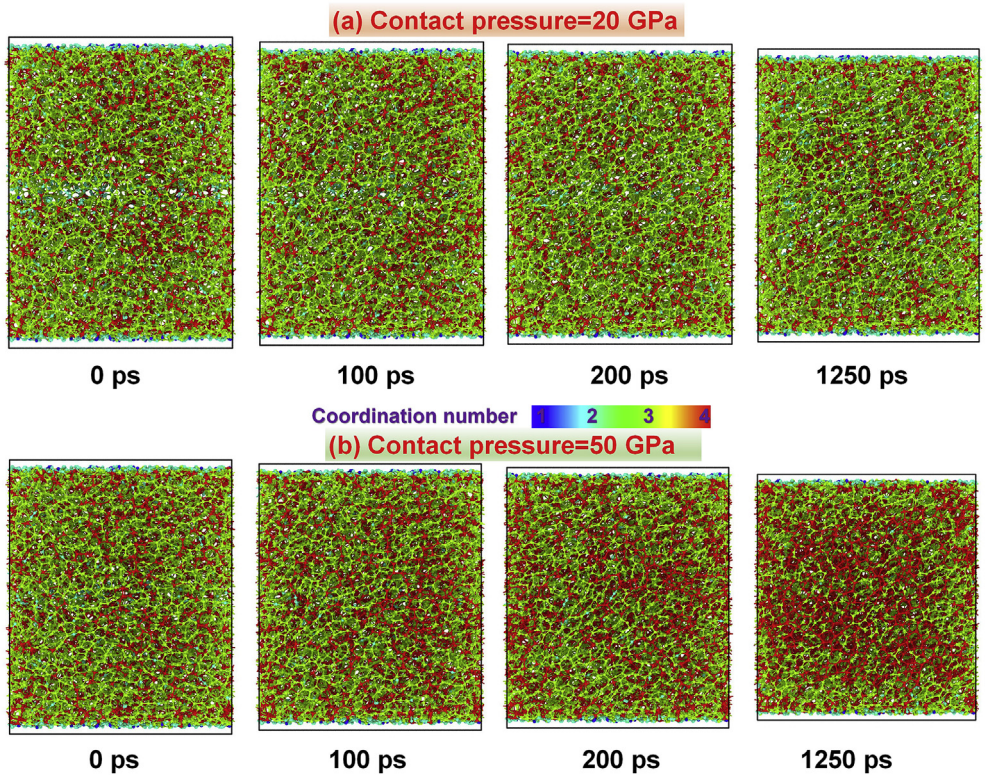

Fig. 9. Morphologies of a-C/a-C friction systems with sliding time under contact pressures of (a) 20 and (b) 50 GPa, respectively.

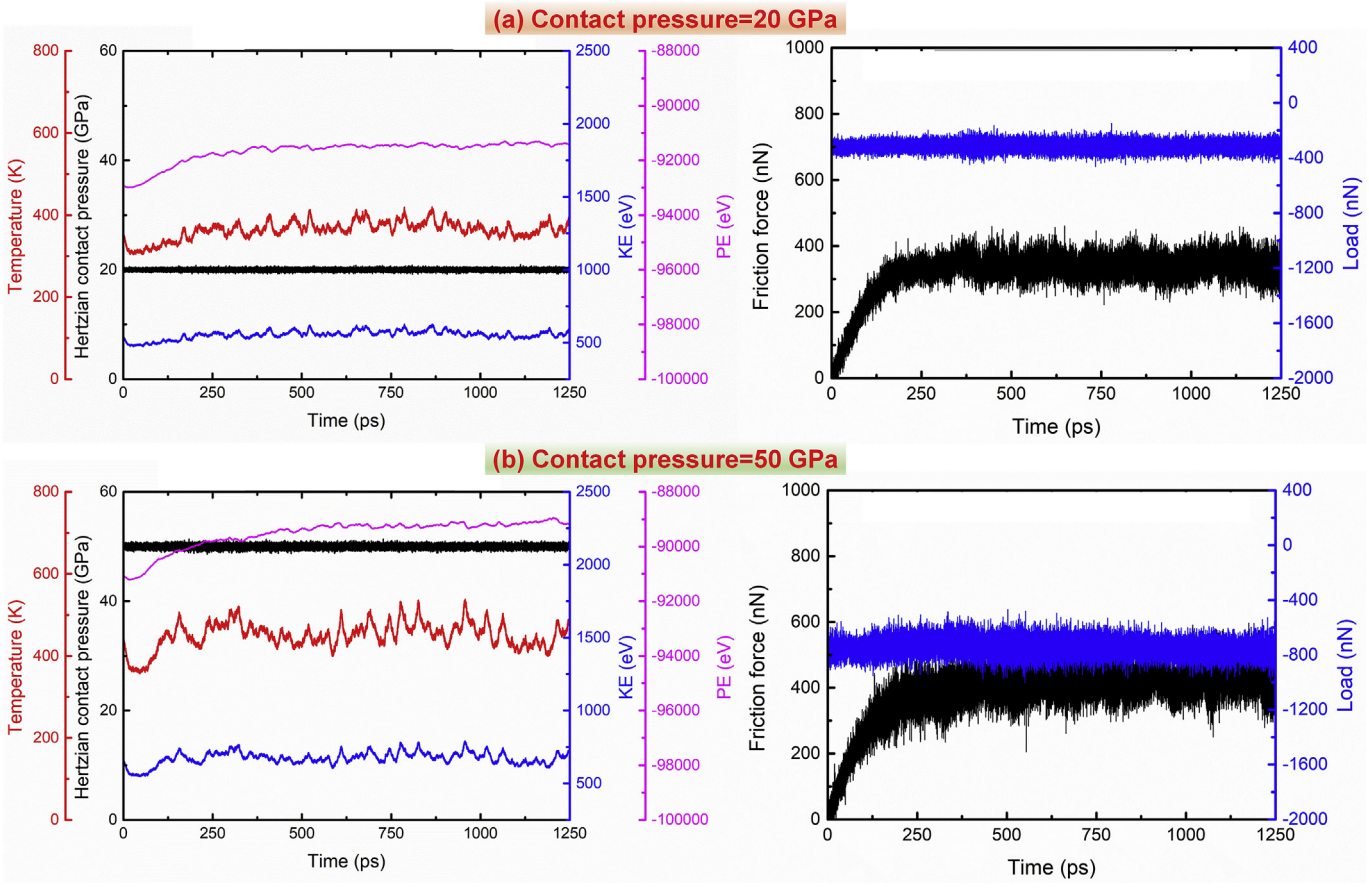

Fig. 10. Contact pressure, temperature, KE, PE, friction force, and load curves with sliding time under contact pressures of (a) 20 and (b) 50 GPa, respectively.

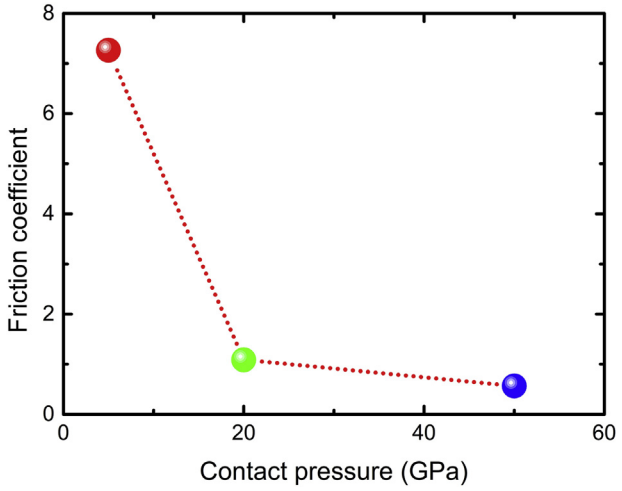

Fig. 11. Friction coefficient as a function of contact pressure after friction process.

coefficient of a-C was sensitive to the ratio of vacuum pressure to sliding velocity. Similarly, the friction coefficient and hybridization structure including sp^2 and sp against the P/v values are also plotted, as given in Fig. 14b. The s-hybridized structure is also considered, despite the very low fraction. It displays a mixed pattern of P/v dependence of friction coefficient, indicating that the suitable selection for contact pressure and sliding velocity is required for low friction, which highly coincides with previous experiment [14]. The change of friction coefficient with P/v values has a similar trend to that of the sp^2 fraction at the interface. However, the friction behavior of a-C films can be clarified by the passivation state of sliding interface without taking into account the graphitization of a-C structure as follows.

a. The change of friction coefficient with P/v values in Fig. 14b is similar to those of un-passivated bonds including sp^2, sp, and s. Under the low P/v conditions (0.167 for 5 GPa–30 m/s, 0.5 for 5 GPa–10 m/s), due to the short time for heat diffusion caused by higher sliding frequency and weak interfacial interaction caused by low contact pressure, the insufficient passivation of s, sp, and sp^2-hybridized bonds of carbon atoms at the interface exists, leading to the high shearing strength (Fig. 14c) followed by the high friction coefficient. The shearing strength of interface, S, during the steady-state friction process describes as follows [47].

$$\mu = \frac{S}{\sigma} \tag{3}$$

where, S is the shearing strength with the unit of GPa, σ is the Hertzian contact pressure with the unit of GPa.

b. When P/v is 2 (20 GPa–10 m/s) and 5 (50 GPa–10 m/s) separately, although the short time for heat diffusion is also existed, the high contact pressure forces the significant interaction of un-passivated bonds at the interfaces to rehybridize with other dangling bonds, and thus the low fractions of un-passivated bonds are observed (Fig. 14b), bringing slower increase rate of shearing strength (Fig. 14c) than that of contact pressure, and thus accounting for the low friction behavior.

c. A transition in friction coefficient from a low value of 0.57 (50 GPa–10 m/s) to a high value of 7.37 (5 GPa–1 m/s) takes place around 5 GPa/m/s. This transition could also be explained by that the low sliding velocity provides enough time duration for atomic

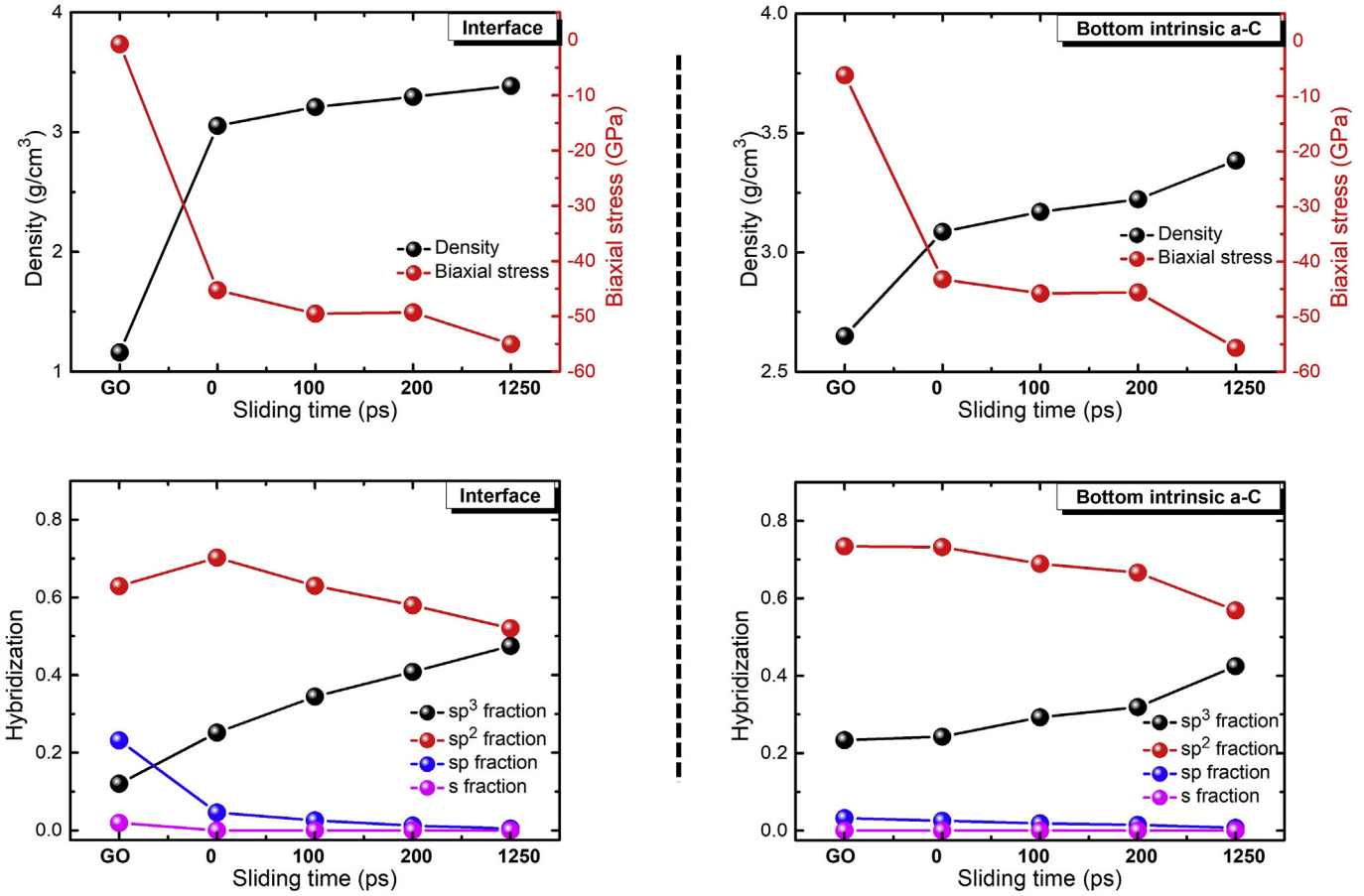

Fig. 12. Evolutions of the density, biaxial stress, and hybridization of interfacial and bottom intrinsic a-C regions with sliding time under the contact pressure of 50 GPa, in which the results after GO are also given for comparison.

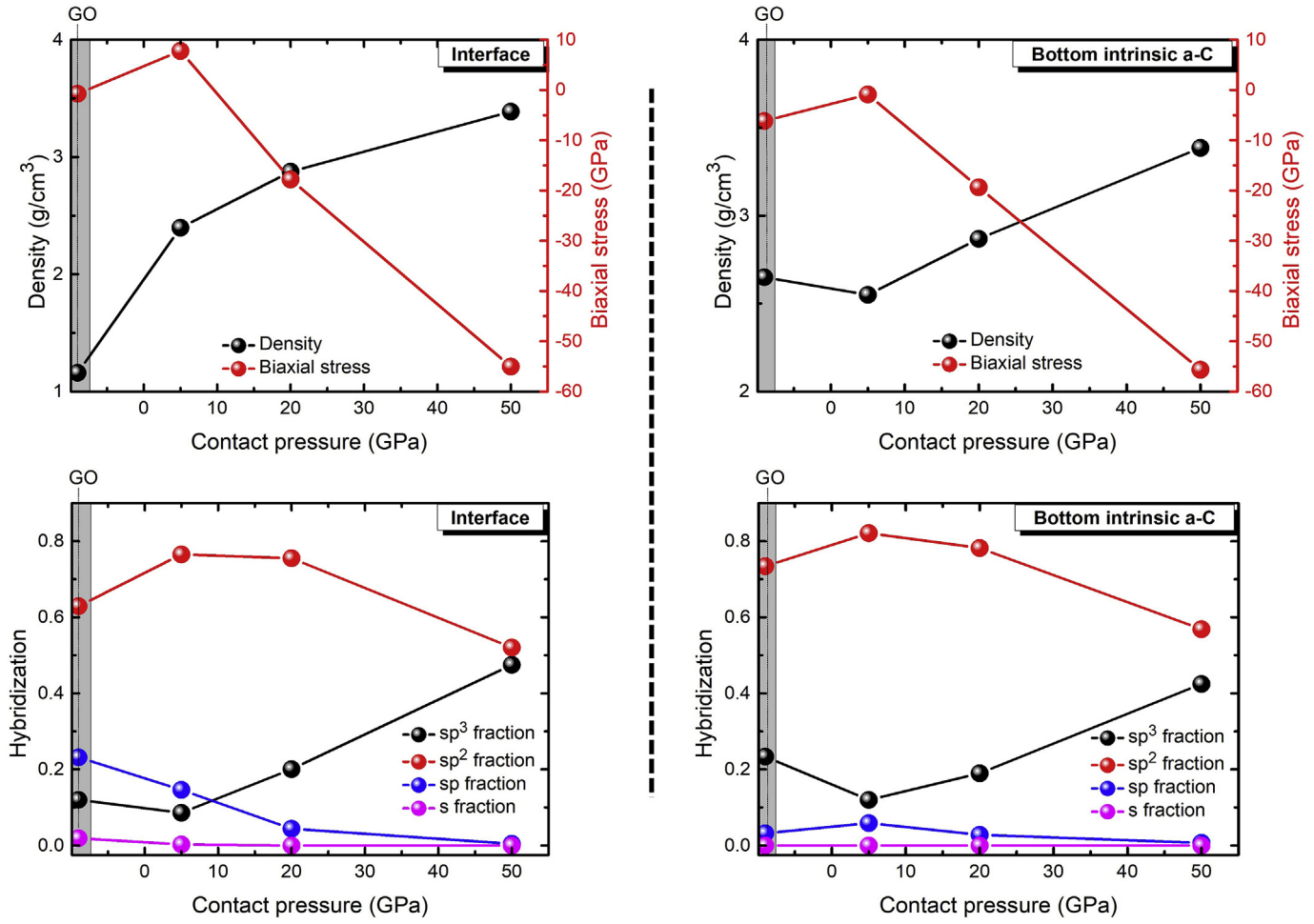

Fig. 13. Dependence of the density, biaxial stress, and hybridization of bottom intrinsic a-C and interfacial regions on contact pressure after friction process, in which the results after GO are also given for comparison.

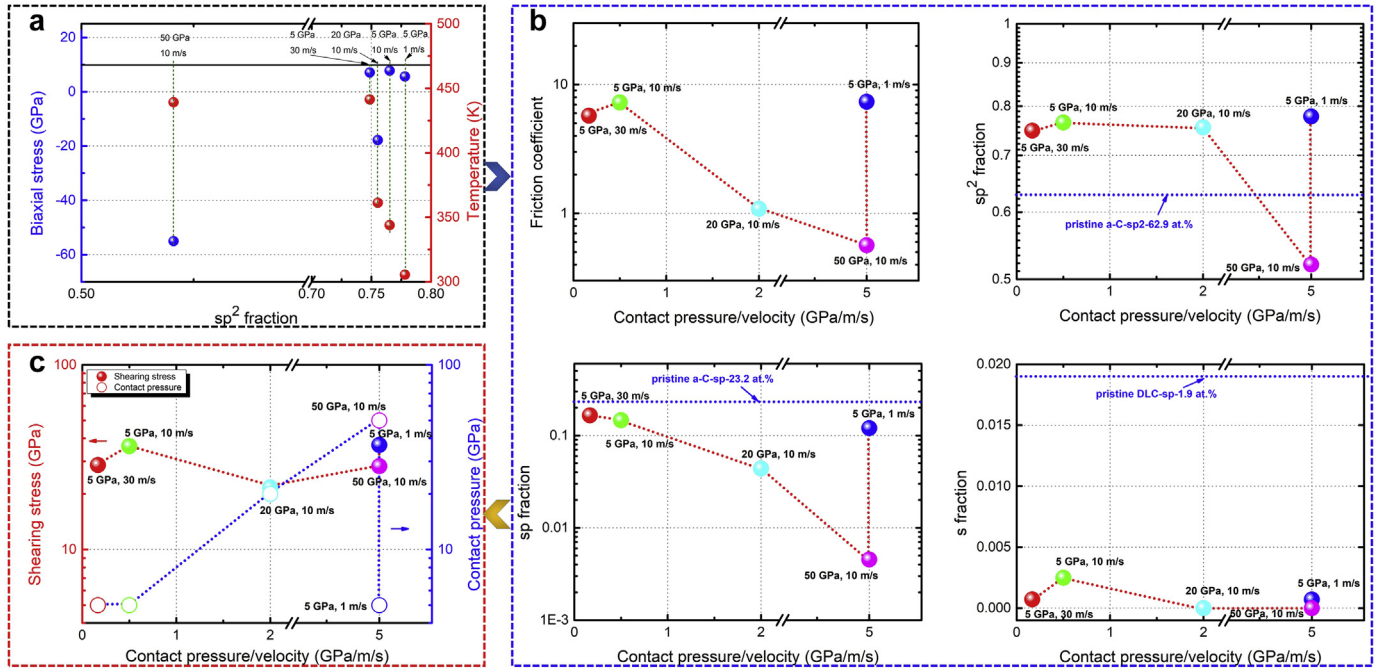

Fig. 14. (a) Relation of biaxial stress, temperature, and sp^2 fraction at the interfacial region. (b) Friction coefficient and hybridized structure (sp^2, sp, and s) versus the ratio of contact pressure to sliding velocity at the interface. (c) Shearing strength and contact pressure versus the ratio of contact pressure to sliding velocity.

interaction, but the low flash temperature rise (306 ± 3 K only) in Fig. 4a induced weak heat diffusion and the low contact pressure also brings the weak interfacial interaction, leading to the insufficient passivation of sp^2, sp, and s bonds (Fig. 14b), which results in the high friction coefficient.

Consequently, both the sliding velocity and contact pressure affect the friction primarily through their effect on the interfacial passivation during the friction process (Fig. 14b), which is highly supported by Cui's experimental result [14], although there are some differences in the friction testing conditions. However, the key evidence about the relation between un-passivated sp^2, sp, s bonds and P/v ratio was not given in previous experiment, because the present characterization technique cannot provide the accurate evaluation of un-passivated carbon bond fractions, while it is completed systematically by the present work from the atomic scale. In addition, we only simulate the nature of intrinsic a-C/a-C friction system in the present simulation under vacuum condition. If the presence of any gaseous reactive species in the simulation box (such as water, oxygen, or hydrogen) are introduced, it can be deduced that the significance of passivation mechanism on friction process should be magnified obviously, which has been proved by experimental [14,48,49] and simulation results [33,50,51]. Future work is necessary to distinguish the potential role of passivating species (oxygen or hydrogen) and intrinsic a-C self-passivation on the friction mechanism.

4. Conclusions

In this study, we performed RMD simulation using ReaxFF to investigate the effect of sliding velocity and contact pressure on the friction behavior of a-C/a-C system in order to explore the related fundamental friction mechanism. Hybridization structure, density, biaxial stress, and friction coefficient were calculated. Results revealed that with increasing the sliding velocity from 1 to 30 m/s or contact pressure from 5 to 50 GPa, the friction coefficient reduced significantly, and when the contact pressure and sliding velocity were fixed at 50 GPa and 10 m/s separately, the minimal friction coefficient of 0.57 is obtained. Compared to the pristine case, the increased sp^2 fraction could be achieved, but it mainly depended on the applied contact pressure, and this sp^3–to–sp^2 transformation was inspired by the reduction of residual compressive stress in the friction system. Furthermore, the friction coefficient was found to depend on the ratio of contact pressure to sliding velocity, and a higher friction coefficient was accompanied by a higher sp^2 fraction, which agreed well with previous experiment. Although the present results were not in accordance with the character of graphitization-induced low-friction of a-C films, the passivation of sp^2, sp, and s-hybridized carbon bonds at the sliding interface accurately accounted for the friction behavior for a-C/a-C system.

Acknowledgments

This research was supported by the Korea Research Fellowship Program funded by the Ministry of Science and ICT through the National Research Foundation of Korea (2017H1D3A1A01055070), the Nano Materials Research Program through the Ministry of Science and IT Technology (NRF-2016M3A7B4025402), and the National Natural Science Foundation of China (51772307, 51522106).

References

[1] Robertson J. Diamond-like amorphous carbon. Mater Sci Eng R 2002;37:129–281.
[2] Wang Y, Gao K, Zhang B, Wang Q, Zhang J. Structure effects of sp2-rich carbon films under super-low friction contact. Carbon 2018;137:49–56.
[3] Cui L, Zhou H, Zhang K, Lu Z, Wang X. Bias voltage dependence of superlubricity lifetime of hydrogenated amorphous carbon films in high vacuum. Tribol Int 2018;117:107–11.
[4] Wan S, Li D, Zhang G, Tieu AK, Zhang B. Comparison of the scuffing behavior and wear resistance of candidate engineered coatings for automotive piston rings. Tribol Int 2017;106:10–22.
[5] Kim DW, Kim KW. Effects of sliding velocity and normal load on friction and wear characteristics of multi-layered diamond-like carbon (DLC) coating prepared by reactive sputtering. Wear 2013;297:722–30.
[6] Liu Y, Yu B, Cao Z, Shi P, Zhou N, Zhang B, Zhang J, Qian L. Probing superlubricity stability of hydrogenated diamond-like carbon film by varying sliding velocity. Appl Surf Sci 2018;439:976–82.
[7] Igartua A, Berriozabal E, Nevshupa R, Roman E, Pagano F, Nielsen LP, Louring S, Muntada L. Screening of diamond-like carbon coatings in search of a prospective solid lubricant suitable for both atmosphere and high vacuum applications. Tribol Int 2017;114:192–200.
[8] Wu D, Ren S, Pu J, Lu Z, Zhang G, Wang L. A comparative study of tribological characteristics of hydrogenated DLC film sliding against ceramic mating materials for helium applications. Appl Surf Sci 2018;441:884–94.
[9] Ma TB, Hu YZ, Wang H. Molecular dynamics simulation of shear-induced graphitization of amorphous carbon films. Carbon 2009;47:1953–7.
[10] Ma TB, Hu YZ, Xu L, Wang LF, Wang H. Shear-induced lamellar ordering and interfacial sliding in amorphous carbon films: a superlow friction regime. Chem Phys Lett 2011;514:325–9.
[11] Lei B, He L, Yi M, Ran L, Xu H, Ge Y, Peng K. New insights into the microstructure of the friction surface layer of C/C Composites. Carbon 2011;49:4554–62.
[12] Tasdemir HA, Wakayama M, Tokoroyama T, Kousaka H, Umehara N, Mabuchi Y, Higuchi T. Wear behaviour of tetrahedral amorphous diamond-like carbon (ta-C DLC) in additive containing lubricants. Wear 2013;307:1–9.
[13] Chen X, Zhang C, Kato T, Yang X, Wu S, Wang R, Nosaka M, Luo J. Evolution of tribo-induced interfacial nanostructures governing superlubricity in a-C:H and a-C:H:Si films. Nat Comm 2017;8:1675.
[14] Cui L, Lu Z, Wang L. Probing the low-friction mechanism of diamond-like carbon by varying of sliding velocity and vacuum pressure. Carbon 2014;66:259–66.
[15] Konicek AR, Grierson DS, Sumant AV, Friedmann TA, Sullivan JP, Gilbert PUPA, Sawyer WG, Carpick RW. Influence of surface passivation on the friction and wear behavior of ultrananocrystalline diamond and tetrahedral amorphous carbon thin films. Phys Rev B 2012;85:155448.
[16] Li X, Wang A, Lee KR. Mechanism of contact pressure-induced friction at the amorphous carbon/alpha olefin interface. npj Comput Mater 2018;4:53.
[17] Kuwahara T, Moras G, Moseler M. Friction regimes of water-lubricated diamond (111): role of interfacial ether groups and tribo-induced aromatic surface reconstructions. Phys Rev Lett 2017;119:096101.
[18] Merkle AP, Erdemir A, Eryilmaz OL, Johnson JA, Marks LD. In situ TEM studies of tribo-induced bonding modifications in near-frictionless carbon films. Carbon 2010;48:587–91.
[19] M'ndange-Pfupfu A, Eryilmaz OL, Erdemir A, Marks LD. Quantification of sliding-induced phase transformation in N3FC diamond-like carbon films. Diam Relat Mater 2011;20:1143–7.
[20] Zhao R, Steiner J, Andreas K, Merklein M, Tremmel S. Investigation of tribological behavior of a-C:H coatings for dry deep drawing of aluminium alloys. Tribol Int 2018;118:484–90.
[21] Srinivasan SG, van Duin ACT, Ganesh P. Development of a ReaxFF potential for carbon condensed phases and its application to the thermal fragmentation of a large fullerene. J Phys Chem 2015;119:571–80.
[22] Tavazza F, Senftle TP, Zou C, Becker CA, van Duin ACT. Molecular dynamics investigation of the effects of tip-substrate interactions during nanoindentation. J Phys Chem C 2015;119:13580–9.
[23] Tersoff J. New empirical approach for the structure and energy of covalent systems. Phys Rev B 1988;37:6991–7000.
[24] Erhart P, Albe K. Analytical potential for atomistic simulation of silicon, carbon, and silicon carbide. Phys Rev B 2005;71:035211.
[25] Brenner DW, Shenderova OA, Harrison JA, Stuart SJ, Ni B, Sinnott SB. A second-generation reactive empirical bond order (REBO) potential energy expression for hydrocarbons. J Phys Condens Matter 2002;14:783–802.
[26] Stuart SJ, Tutein AB, Harrison JA. A reactive potential for hydrocarbons with intermolecular interactions. J Chem Phys 2000;112:6472–86.
[27] Plimpton S. Fast parallel algorithms for short-range molecular dynamics. J Comp Phys 1995;117:1–19.
[28] Li X, Wang A, Lee KR. Comparison of empirical potentials for calculating structural properties of amorphous carbon films by molecular dynamics simulation. Comp Mater Sci 2018;151:246–54.
[29] Berendsen HJC, Postma JPM, van Gunsteren WF, DiNola A, Haak JR. Molecular dynamics with coupling to an external bath. J Chem Phys 1984;81:3684–90.
[30] Ma TB, Wang LF, Hu YZ, Li X, Wang H. A shear localization mechanism for lubricity of amorphous carbon materials. Sci Rep 2014;4:3662.
[31] Zilibotti G, Corni S, Righi MC. Load-induced confinement activates diamond lubrication by water. Phys Rev Lett 2013;111:146101.
[32] Bai S, Murabayashi H, Kobayashi Y, Higuchi Y, Ozawa N, Adachi K, Martin JM, Kubo M. Tight-binding quantum chemical molecular dynamics simulations of the low friction mechanism of fluorine-terminated diamond-like carbon films. RSC Adv 2014;4:33739–48.
[33] Chen YN, Ma TB, Chen Z, Hu YZ, Wang H. Combined effects of structural transformation and hydrogen passivation on the friction behaviors of hydrogenated amorphous carbon films. J Phys Chem C 2015;119:16148–55.
[34] Li K, Zhang H, Li G, Zhang J, Bouhadja M, Liu Z, Skelton AA, Barati M. ReaxFF molecular dynamics simulation for the graphitization of amorphous carbon: a parametric study. J Chem Theory Comput 2018;14:2322–31.
[35] Li X, Guo P, Sun L, Zuo X, Zhang D, Ke P, Wang A. Ti/Al co-doping induced residual stress reduction and bond structure evolution of amorphous carbon films: an experiment and ab initio study. Carbon 2017;111:467–75.

[36] Kresse G, Furthmüller J. Efficiency of ab initio total energy calculations for metals and semiconductors using plane-wave basis set. Comp Mater Sci 1996;6:15–50.
[37] Kresse G, Furthmüller J. Efficient iterative schemes for ab initio total-energy calculations using a plane-wave basis set. Phys Rev B 1996;54:11169–86.
[38] Li L, Xu M, Song W, Ovcharenko A, Zhang G, Jia D. The effect of empirical potential functions on modeling of amorphous carbon using molecular dynamics method. Appl Surf Sci 2013;286:287–97.
[39] Koivusaari KJ, Rantala TT, Leppävuori S. Calculated electronic density of states and structural properties of tetrahedral amorphous carbon. Diam Relat Mater 2000;9:736–40.
[40] McCulloch DG, McKenzie DR, Goringe CM. Ab initio simulation of the structure of amorphous carbon. Phys Rev B 2000;61:2349–55.
[41] Marks N, Cooper N, McKenzie D, McCulloch D, Bath P, Russo S. Comparison of density-functional, tight-binding, and empirical methods for the simulation of amorphous carbon. Phys Rev B 2002;65:075411.
[42] Ferrari AC, Libassi A, Tanner BK, Stolijan V, Yuan J, Brown LM, Rodil SE, Kleinsorge B, Robertson J. Density, sp^3 fraction, and cross-sectional structure of amorphous carbon films determined by x-ray reflectivity and electron energy-loss spectroscopy. Phys Rev B 2000;62:11089–103.
[43] Fallon PJ, Veerasamy VS, Davis CA, Robertson J, Amaratunga GAJ, Milne WI, Koskinen J. Properties of filtered-ion-beam-deposited diamondlike carbon as a function of ion energy. Phys Rev B 1993;48:4777–82.
[44] Hutchings I, Shipway P. Tribology: friction and wear of engineering materials. second ed. Butterworth-Heinemann; 2017.
[45] McKenzie DR, Muller D, Pailthorpe BA. Compressive-stress induced formation of thin-film tetrahedral amorphous carbon. Phys Rev Lett 1991;67:773–6.
[46] Li H, Xu T, Wang C, Chen J, Zhou H, Liu H. Humidity dependence on the friction and wear behavior of diamondlike carbon film in air and nitrogen environments. Diam Relat Mater 2006;15:1585–92.
[47] Bowden FP, Tabor D. The friction and lubrication of solids. Oxford: Clarendon; 1964.
[48] Eryilmaz OL, Erdemir A. On the hydrogen lubrication mechanism(s) of DLC films: an imaging TOF-SIMS study. Surf Coat Technol 2008;203:750–5.
[49] Guo P, Geng Z, Lu Z, Zhang G, Wu Z. Probing the lubrication mechanism of rough diamond-like carbon films against silicon nitride under water. Tribol Int 2018;128:248–59.
[50] Wang Y, Xu J, Ootani Y, Bai S, Higuchi Y, Ozawa N, Adachi K, Martin JM, Kubo M. Tight-binding quantum chemical molecular dynamics study on the friction and wear processes of diamond-like carbon coatings: effect of tensile stress. ACS Appl Mater Interfaces 2017;9:34396–404.
[51] Bai S, Onodera T, Nagumo R, Miura R, Suzuki A, Tsuboi H, Hatakeyama N, Takaba H, Kubo M, Miyamoto A. Friction reduction mechanism of hydrogen- and fluorine-terminated diamond-like carbon films investigated by molecular dynamics and quantum chemical calculation. J Phys Chem C 2012;116:12559–65.